

STRUCTURAL PROTEIN-BASED FLEXIBLE WHISPERING GALLERY MODE RESONATORS

Huzeyfe Yılmaz^{1,*}, Abdon Pena-Francesch^{2,*}, Robert Shreiner², Chester J. Szwejkowski³,
Huihun Jung², Patrick Hopkins³, Şahin Kaya Özdemir¹, Lan Yang¹, Melik C. Demirel^{2,4}

¹ Electrical and Systems Engineering Department, Washington University, St. Louis, MO 63130

² Department of Engineering Science and Mechanics, Pennsylvania State University, University
Park, PA, 16802

³ Department of Mechanical and Aerospace Engineering, University of Virginia, Charlottesville,
VA 22904

⁴ Materials Research Institute and Huck Institutes of Life Sciences, Pennsylvania State
University, University Park, PA, 16802

*These authors contributed equally

Corresponding Authors E-mails: LY yang@seas.wustl.edu, ŞKÖ ozdemir@wustl.edu, MCD
mdemirel@engr.psu.edu

Abstract

Nature provides a set of solutions for photonic structures that are finely tuned, organically diverse and optically efficient. Exquisite knowledge of structure-property relationships in proteins aids in the design of materials with desired properties for building devices with novel functionalities, which are difficult to achieve or previously unattainable. Recent bio-inspired photonic platforms made from proteinaceous materials lay the groundwork for many functional device applications, such as electroluminescence in peptide nucleic acids¹, multiphoton absorption in amyloid fibers² and silk waveguides and inverse opals³⁻⁵. Here we report whispering-gallery-mode (WGM) microresonators fabricated entirely from semi-crystalline structural proteins (i.e., squid ring teeth, SRT, from *Loligo vulgaris* and its recombinant, and silk from *Bombyx mori*) with unconventional thermo-optic response. We present a striking example of how small modifications at the molecular level lead to structural changes and alter macroscopic properties of proteins by demonstrating the variation in thermo-optic response as a function of crystallinity. We demonstrated waveguides, add-drop filters and flexible resonators as first examples of energy-efficient, highly flexible, biocompatible and biodegradable protein-based photonic devices. Optical switching efficiency in these devices is over thousand times greater than the values reported for Silica WGM resonators. This work opens the way for designing energy efficient functional photonic devices using structure-property relationships of proteins.

The ability to manipulate and control light flow and light–matter interactions using whispering-gallery-mode (WGM) resonators has created significant interest in various fields of science, including but not limited to biosensing^{6,7} and detection^{8,9}, cavity-QED¹⁰, optomechanics¹¹, and parity-time symmetric photonics¹². WGM resonators are currently manufactured using microelectronics technologies with conventional materials such as silica¹³, silicon¹⁴, and silicon nitride¹⁵. However, recent developments in optical technologies have revealed the strong need for developing soft, biocompatible, and biodegradable photonic devices and photonic structures with novel functionalities that cannot be attained with current optical materials¹⁶. Towards this aim, all-polymer¹⁷ and polymer-coated silica WGM resonators¹⁸, as well as silica WGM resonators encapsulated in low-index polymers¹⁹ have been fabricated using conventional and commercially available polymers, such as polydimethylsiloxane (PDMS) and polystyrene (PS) to address the need for flexible structures. However, their molecular morphology (e.g., crystallinity) is limited by existing synthetic approaches. Nature, on the other hand, has optimized proteins through millions of years of evolution to provide diverse materials with complex structures. Thus studying structural proteins at the molecular level will help us in our endeavor for efficiently designing diverse materials, which are finely tunable, flexible, biodegradable, and have physical properties and functionalities different or superior to those currently present in conventional materials. This will also enable the production of functional devices with less chemical processing and energy consumption, addressing growing environmental concerns.

In this Letter, we studied thermo-optic properties of whispering-gallery-mode microresonators fabricated solely from semi-crystalline structural proteins, and elucidated their structure-property relationships for developing energy efficient devices. We fabricated microresonators using silk (**Fig. 1a**), native SRT (**Fig. 1b**), and recombinant SRT (**Fig. 1c**) to study the structure-property relation and demonstrate the possibility of building flexible all-protein functional photonic devices. All-protein microtoroid WGM resonators were fabricated using a molding and solution casting technique (**Fig. S1**). From initial silica templates fabricated as previously described²⁰, we prepared polydimethylsiloxane (PDMS) negative molds for solution casting of the proteins. The microtoroid structures were then manufactured by filling the respective protein solutions into the corresponding PDMS molds. Light from a tunable laser was evanescently coupled in and out of the fabricated resonators through a tapered optical fiber to measure their resonance properties.

Structural proteins are characterized by long-range ordered molecular secondary structures (e.g., β -sheets, coiled coils, or triple helices) that arise due to highly repetitive primary amino acid sequences within the proteins. These features promote the formation of structural hierarchy via self-assembly. Silk and SRT are semi-crystalline structural proteins, which are flexible, biodegradable, and thermally and structurally stable materials. Semi-crystalline morphology of these proteins, which emanates from their β -sheet secondary structures, is ideal for tunability of their physical properties. Degummed silk and SRT protein complexes are composed of several proteins varying in molecular weight (e.g., 10-55 kDa)²¹. Although optical properties do not vary with polydispersity in molecular weight due to linear dielectric response or statistically driven size, they may change in special cases due to cooperative non-linear response or thermal effects. Therefore, a recombinant SRT (Rec) protein with unique molecular weight (i.e., 18 kDa) is also selected to create a monodisperse material, providing advantages in thermo-optical response as well as mechanical properties (e.g., melt viscosity, tensile strength, toughness)²². A combination of RNA-sequencing, protein mass spectroscopy, and bioinformatics tools (i.e., transcriptome assembly) was performed to produce 18 kDa recombinant SRT protein²² (**Fig. 1d**). Both silk and SRT molecular structure provides a rich architecture that can microphase separate to form amorphous Gly-rich and crystalline β -sheet regions with domain size of 2-3 nm. However, SRT proteins show considerable diversity (variable AVSTH-rich) in their crystal-forming sequences²³, while silk protein is made up of highly ordered β -sheet stacks containing oligomers of GAGAGS repeats²⁴. Rec, SRT and silk proteins were analyzed using X-ray diffraction (XRD), which showed that cast silk sample has the lowest crystallinity, and SRT protein had lower crystallinity compared to Rec protein at room temperature (**Fig. S3a-c**). Rec, SRT and silk proteins were also analyzed using infrared spectroscopy (FTIR). Amide regions of FTIR data also confirm that the crystalline regions are composed of β -sheets and α -turns (**Fig. S3e-g**). **Figures 1e** present an example protein-based WGM resonator and related transmission spectra of in the 977 nm band. The quality factors of these proteinaceous WGM resonators ranged from 10^5 to 10^6 (**Fig. S2**).

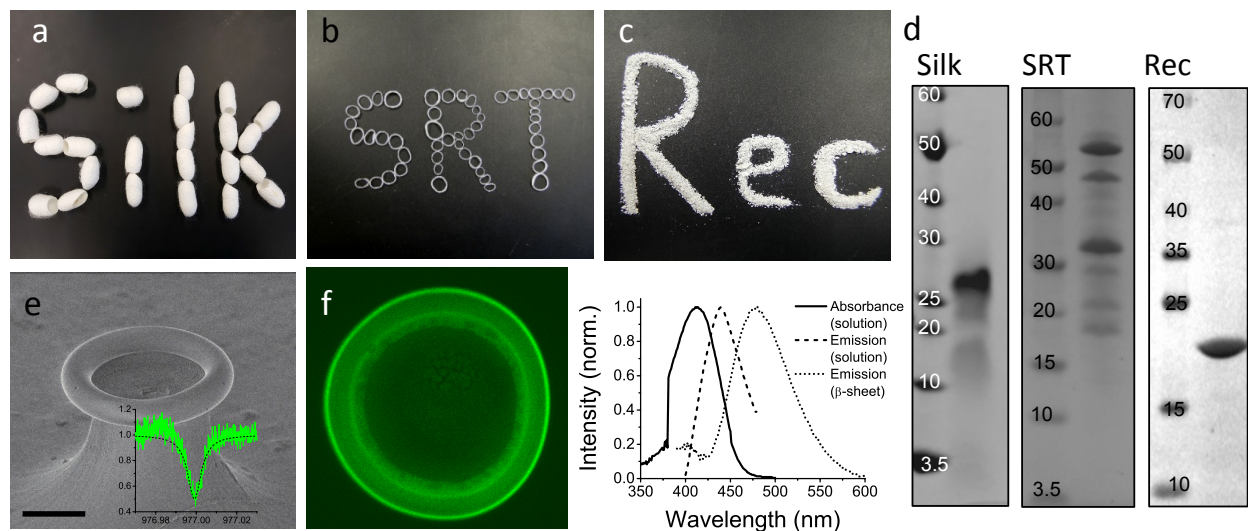


Figure 1. All-protein whispering-gallery-mode (WGM) microresonators. (a)-(c) Optical images of silk cocoons, SRT rings and recombinant SRT (rec) powder proteins. (d) SDS-Page shows protein molecular weight varying between 10-30 kDa for cast silk, 15-55 kDa for native SRT, and 18 kDa for recombinant SRT. (e) Scanning electron microscope (SEM) image of a WGM resonator fabricated from SRT protein (Scale bar 20 μ m). Insets present typical transmission spectra of WGM resonances in the 977 nm. (f) Green fluorescence emission from an all-SRT chip, which is doped with 1 mM of thioflavin-T (ThT) dye confirming the large red-shift due its binding to β -sheets in the protein. Absorbance and emission spectra of ThT dye. The absorption peak of ThT in solution is at 412 nm. When it is free in a solution, it emits light at 438 nm, and when it is bound to β -sheets in proteins it emits at 482 nm.

We probed the nano-crystalline regions in these structural proteins, delineated by anti-parallel β -sheets, using fluorescent microscopy. We selected a fluorescent dye, thioflavin-T (ThT), which binds specifically to the β -sheets, but does not bind to amorphous polypeptides²⁵. When ThT dye binds to β -sheets, it undergoes a characteristic red shift of its excitation/emission spectrum (**Fig. 1f**) that may be selectively excited with blue light at 450 nm, resulting in a green fluorescence signal with maximum at 482 and extending to 570 nm. We prepared an all-SRT chip with microresonators, an SRT-coated silica microresonator, a silica resonator partially coated with SRT, and a PDMS chip with microresonators (see Supplementary Information, **Fig. S4**) to test selective binding of ThT dye. The green fluorescence emitted by the all-SRT chip when exposed to blue light is indicative of a large red-shift in emission due to the binding of the ThT dye to β -sheets (**Fig. 1f**).

We experimentally determined the thermo-optic coefficient of silk and SRT proteins by monitoring the resonant wavelength of a WGM resonator while the temperature of the all-protein

chip substrate was varied (**Fig. 2a**). We also chemically treated SRT resonator (i.e., sample kept in methanol for 4 hours) and measured the resonant wavelength shift as a function of temperature. For all resonators, we observed that the resonant wavelengths, λ , experience a blue shift (i.e., decrease in wavelength) as the temperature was increased (**Fig. 2a**), i.e., $d\lambda(n,r)/dT < 0$. Subsequently, using the measured parameters in the relation $1/\lambda \, d\lambda(n,r)/dT = 1/n \, dn/dT + 1/r \, dr/dT$, where T is temperature, n is the refractive index, $1/r \, dr/dT$ is the linear thermal expansion coefficient, and r is the radius of the resonator, we calculated the normalized thermo-optic coefficients $1/n \, dn/dT$ of silk, SRT and Rec proteins at 1420 nm wavelength.

The thermo-optic coefficient can be written as a function of density change and temperature change, $dn/dT = (\partial n/\partial \rho)_T (\partial \rho/\partial T) + (\partial n/\partial T)_\rho = -(\rho \partial n/\partial \rho)_T \alpha + (\partial n/\partial T)_\rho$, where ρ is the density, α is the coefficient of thermal expansion. The first term on the right side of the equation is the volume-dependent thermal response, which is related to thermal expansion. The second term, on the other hand, is the volume independent thermal response that is solely determined by the electronic structure of the material. We measured the thermal expansion coefficient for all protein samples (i.e., $-95 \times 10^{-6} \pm 7 \times 10^{-6} \text{ K}^{-1}$ for SRT proteins and $-300 \times 10^{-6} \pm 10 \times 10^{-6} \text{ K}^{-1}$ for silk). Apparent negative thermal expansion coefficient is not surprising for structural proteins. For rubbery materials, thermal expansion coefficient depends on the strain. In general, the total expansion is obtained by adding the expansion coefficient, α , to the unstressed material, $\alpha' = \alpha - \varepsilon/T$. For example, a natural rubber stretched three times of its length gives a contribution of about -10^{-2} K^{-1} at room temperature²⁶. Similarly, silk shrinks significantly in size when hydrated due to inter-domain stresses (e.g. supercontraction of amorphous domains) in the native form²⁷.

The volume independent index change, $(\partial n/\partial T)_\rho$, is too small for conventional polymers. Zhang *et al.* showed a linear relationship between dn/dT and α values ignoring the volume independent term²⁸ for conventional polymers. However, volume independent index change for structural proteins should not be ignored since crystalline β -sheets domains act as grain boundaries and hence significantly contribute to the optical properties (e.g., reflectivity). For structural proteins, we show below that volume independent index change term has negative sign ($\partial n/\partial T < 0$), leading to a stronger negative thermo-optic response.

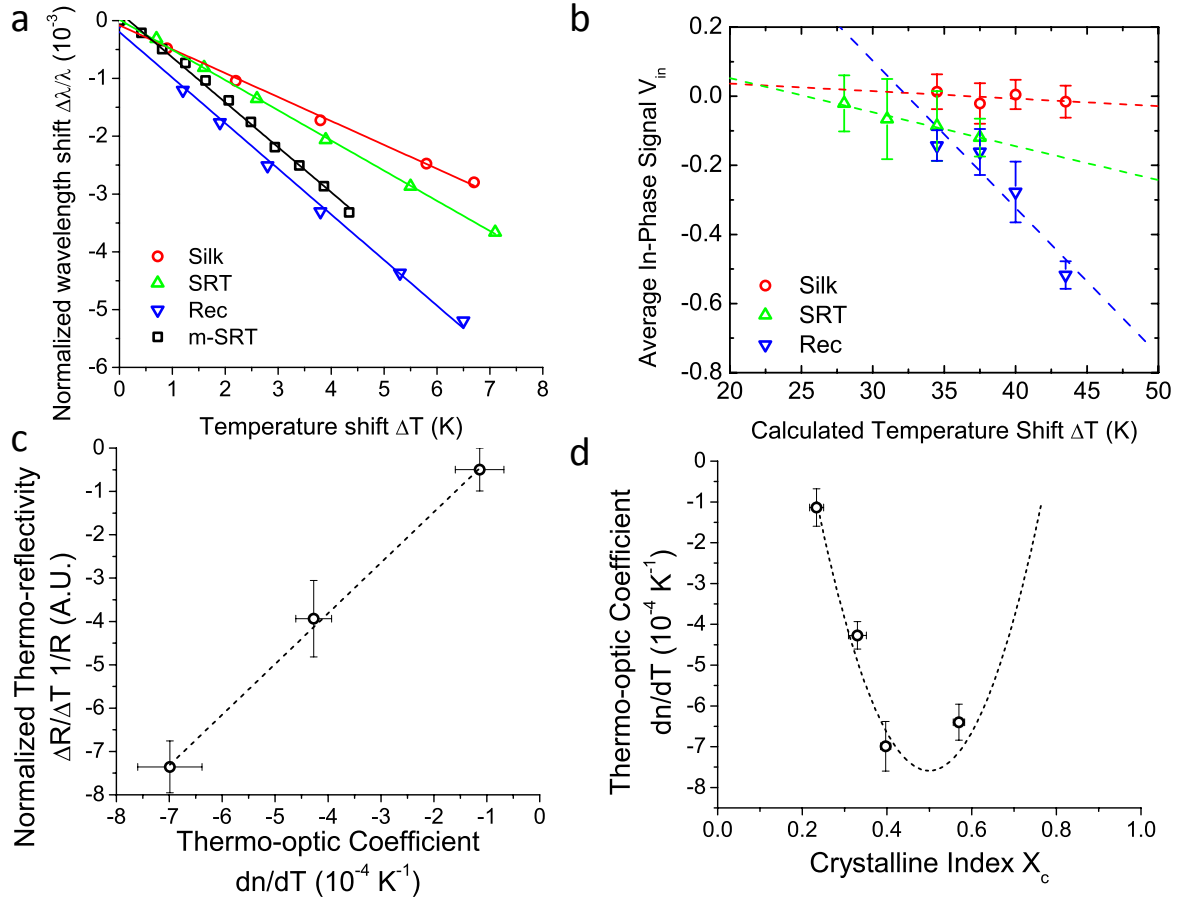


Figure 2. Structure-property relation probed in all-protein whispering-gallery-mode microresonators.

(a) The temperature dependence of the refractive indices of the respective protein-based WGM resonators made of SRT, Silk, recombinant SRT (Rec), and methanol treated SRT (m-SRT). (b) Average in phase signal (V_{in}) due to a heating event from a pump laser pulse as a function of the temperature is representative of the change in reflectivity (R) due to a change in temperature. (c) The normalized thermo-reflectivity increases linearly with the thermo-optic coefficient. The thermo-reflectivity is calculated as $(1/R) (dR/dT) = (\sqrt{2}/GQ)[V_{in}/(\Delta TV_0)]$, where G is the gain of the preamplifier, Q is the quality factor of the circuit, V_0 is the average dc voltage generated by the photodiode detector from pump-probe experiments. The slope of the dashed line is ~ 1.2 , which agrees well with the theoretical prediction of 1.4 (See Supplementary Information) (d) Effect of the crystallinity index on the thermo-optic coefficient measured by all-protein WGM resonators. Methanol treated SRT has increased crystallinity (e.g., X_c increased from 0.34 to 0.58, Fig S3d and S3g). The dashed line shows theoretical prediction for thermo-optic coefficient (e.g., $dn/dT \sim [X_c (1 - X_c)]$) as a function of crystallinity.

We measured the relative magnitude and sign of the volume independent thermo-optic coefficient, $(\partial n/\partial T)_\rho$, using picosecond pump-probe transient absorption measurements (**Fig. 2b**). The pump is used to trigger a rapid thermal process in the sample and the probe beam is used to examine the excited relaxation dynamics and energy changes of excited volume. The temporal evolution of this process is monitored by varying the relative delay time between the pump and probe pulses. While the rapid absorption of the pump pulse leads to both temperature changes and thermal expansion, these signatures of the optical changes of the sample are separable in the time domain²⁹. The characteristic signatures of the temporal thermal response are a rapid exponential decay in ~ 2 ps after laser absorption, representing nonequilibrium redistribution and coupling among thermal carriers, followed by a slower exponential decay, representing the change in the absorption of the sample that is linearly related to temperature (i.e., diffusive thermal transport)³⁰. Our measurements are performed outside the picosecond interval, which also ensures that our measurements do not capture any non-linear optical effects from simultaneous pump and probe absorption in the sample. Using a transmission geometry to detect the transient absorption changes³¹, our measurements on three different structural proteins are then related to the volume independent term in thermo-optic coefficient, as described in the Supplementary Information. (**Fig. S5 a-c**) We benchmark our measurements and analysis using a thin gold film, as the thermo-optic coefficients of gold films have been extensively characterized³² (**Fig. S5d**). Correlation between thermo-optic coefficient and thermorefectivity, which is measured by picosecond pump-probe transient absorbance, shows a linear trend (**Fig. 2c**).

Plotting the thermo-optic coefficients calculated from the experimental data for the tested proteins as a function of crystallinity revealed that the thermo-optic coefficient becomes more negative with increasing crystallinity index of the protein (**Fig. 2d**). Considering the Fresnel and Beer laws (see Supplementary Information), an analytical relationship can be derived $dn/dT = [c \pi r(n+1)^3 \propto / 2(n-1)] X_c (1 - X_c)$, where c is the extinction coefficient, and X_c is the crystallinity index (**Fig 2d**), which agrees well with the experimental data. Since the thermo-optic coefficient is used for dynamic control of refractive index in photonic and electronic devices, its tunability is essential for photonic technologies.

By coupling proteinaceous WGM resonators to two separate fiber-taper waveguides, we fabricated add-drop filters (**Fig. 3a**) that are frequently integrated in optical communication architectures (such as optical filters, multiplexers and routers), as well as used as schemes for high performance optical sensing devices. As seen in **Fig. 3b**, the add-drop filter routed the light from the input waveguide to the drop port in the second waveguide when the wavelength of the light coincided with the resonance wavelength of the SRT resonator. Non-resonant light passed through the input waveguide to the transmission port. The dip in the transmission port and the peak in the drop port seen in **Fig. 3b** clearly confirm that the SRT add-drop filter performed its function with an add-drop efficiency of 51%, which may be further increased by more careful setting of the waveguide-resonator coupling and by decreasing scattering losses. We also produced proteinaceous waveguides (**Fig. 3c**) using electro-spinning (e-spin) technique (**Fig. S6**). Engaging a single protein fiber to a silica fiber taper via van der Waals attractions, we achieved evanescent coupling of light from the silica fiber taper to the protein fiber, clearly demonstrating the waveguiding capability of proteinaceous fibers. The flexible nature of these protein-based WGM resonators is shown in **Fig. 3d**, where the soft base of the WGM microresonators is bent in a bowed shape. This characteristic enables significant bending on a macroscopic scale (see inset). We performed three-point bending dynamic mechanical analysis (DMA) for the recombinant and native SRT as well as silk films to quantitatively describe the flexibility of the fabricated photonic microstructures (**Fig. 3d-inset**). The load-deflection curve shows similar bending modulus (~ 1 GPa) for all films. **Figure 3e** shows bending of the protein substrate as a function of the wavelength of the recombinant SRT resonator. The resonance frequency did not change as the strain in the substrate increased (**Fig. 3e-inset**), which is an important attribute of flexible protein resonators for opto-mechanics applications.

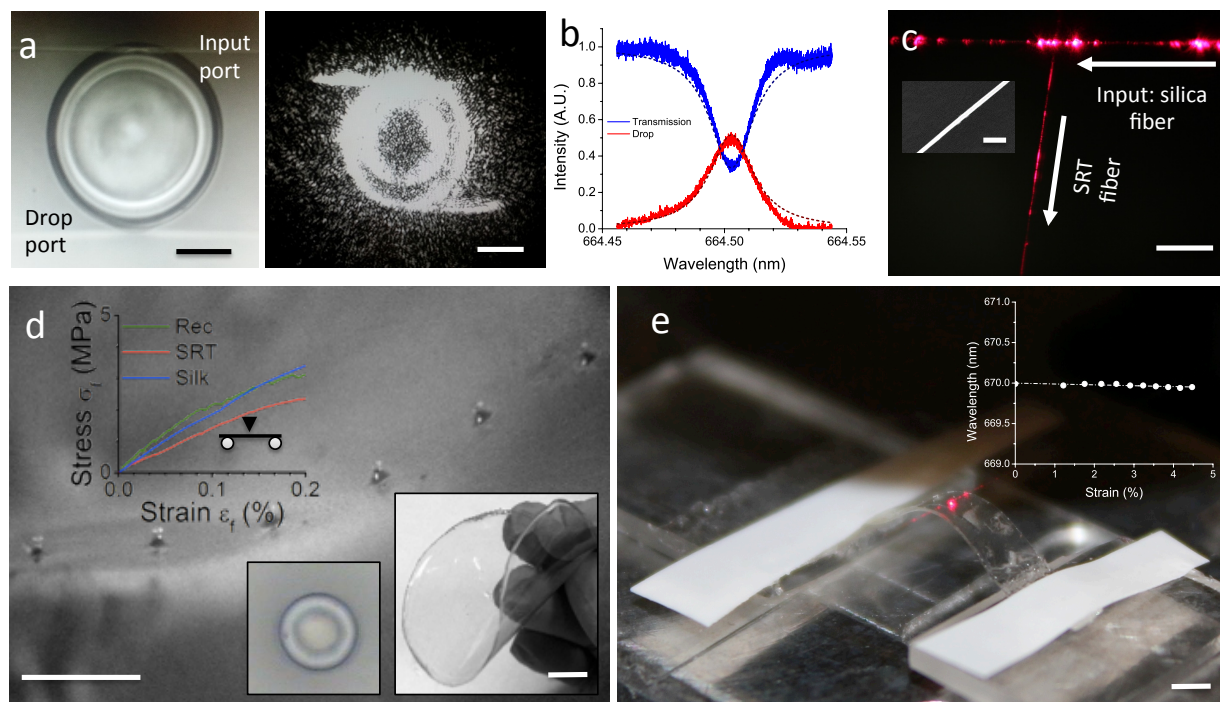


Figure 3. Device examples of semi-crystalline proteins. (a-b) An all-SRT microtoroid resonator with two coupling tapered-fiber waveguides forming an add-drop filter. Transmission spectrum at 667 nm band shows a resonant dip in the transmission port and a resonance peak in the drop port (scale bars 20 μ m). (c) Light transmission through a fiber waveguide prepared from recombinant SRT by electrospinning. Coupling of laser light into the protein fiber was done using a silica tapered fiber (scale bar 50 μ m). (d) Flexibility of the substrate (scale bar 1 cm) and of the WGM resonators fabricated from SRT (scale bar 1 mm). Inset presents the results of dynamic mechanical analysis (DMA) measurements used to quantify the bending of native and recombinant SRT and of silk films. (e) Wavelength measurements of flexible substrate as a function of strain (inset) show stable resonance in the protein resonator.

Finally, in order to utilize the strong thermo-optic response of structural proteins, we constructed an all-optical on/off switch using protein-based WGM structure (**Fig. 4a**) where a pump laser (1450nm band) controlled the transmission of a probe light (980 nm band) via the thermal response of the protein. First, two resonance modes were identified (i.e., 1451.7 nm and 974.8 nm). We fixed the wavelength of the probe laser to the probe resonance wavelength where the normalized transmission of the probe along the fiber was set to zero. Then we fixed the wavelength of the pump laser slightly detuned from the pump resonance where the normalized transmission of the pump through the fiber taper was set to unity. Using a square signal, we then tuned the pump laser wavelength to the pump mode wavelength where the normalized transmission of the pump became zero, which in turn heated the cavity and shifted the probe resonance wavelength, effectively moving the probe laser out of resonance with the protein microresonator and the normalized probe transmission became unity, which completed the all-

optical switching with an SRT protein microtoroid (**Fig. 4b**). Repeating this experiment for various input powers, we found that the minimum power to perform switching with 12 dB isolation is only 1.6 μW where the circulating power was 143 μW . With silica microtoroid resonators, we obtained 8 dB isolation at 22.75 μW of input power and 223 mW of circulating power. Comparing circulating powers, the protein resonator performs the switching with three orders of magnitude less pump power (**Fig. 4c**). This striking performance is due to the strong thermo-optic coefficients of recombinant SRT protein. Our results show that protein-based photonic devices can be used for low power consumption applications. Moreover, we showed that functional and efficient protein-based photonic devices could be fabricated by tuning their crystallinity at the molecular level, which in turn tunes their thermo-optic response.

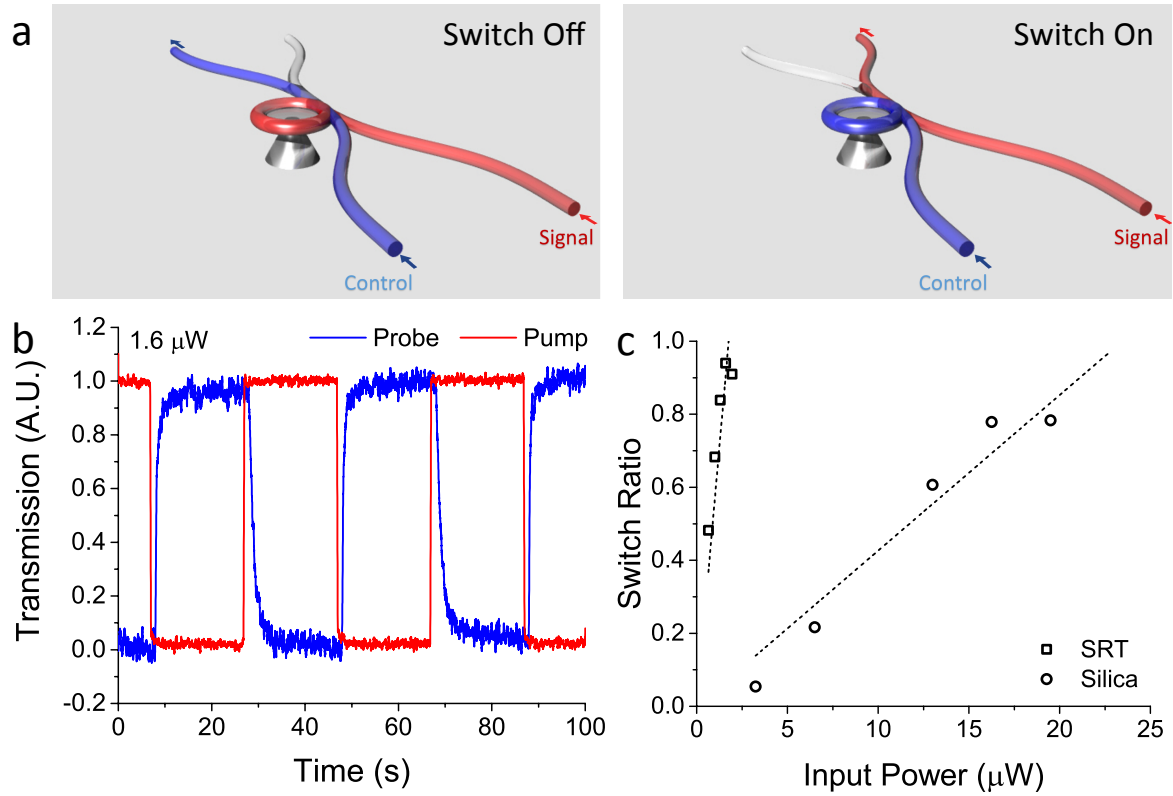


Fig.4 All-optical switch based on thermal shift of WGMs in an all-protein microtoroid resonator. (a) Signal in 980 nm band is initially coupled to the resonator where no light transmits and control light in 1450 nm band is just off resonance (left). When the control light is detuned to the microtoroid resonance, cavity temperature increases and the WGM in the 980 nm band becomes off-resonance (right). (b) Normalized transmission of the signal and the control light at 1.6 μW . (c) Ratio of normalized transmission for various input powers. For a silica microtoroid 22.75 μW of control light is required to perform switching.

In summary, proteinaceous WGM microcavities demonstrated here provide a platform to manipulate photons within microscale volumes at high power efficiency. Our experiments established the link between the crystallinity of the protein-based microresonators and their thermo-optic properties. As illustrated here, protein-based materials could provide the next generation of adaptive photonic structures whose optical, mechanical and thermal properties can be engineered at the molecular level for energy efficient applications in photonics. This approach will also expedite the design, fabrication and synthesis of eco-friendly, recyclable, flexible materials and devices.

Methods

Native squid ring teeth (SRT): European common squid (*Loligo vulgaris*) were caught from the coast of Tarragona (Spain). The squid ring teeth (SRT) were removed from the tentacles, immediately soaked in deionized water and ethanol mixture (70:30 ratio v/v) and vacuum dried in a desiccator.

Expression and characterization of recombinant squid ring teeth (SRT) proteins: The SRT protein family is comprised of SRTs of different size that exhibit different physical properties. Heterologous expression of the smallest (~18 kDa) SRT protein extracted from *Loligo vulgaris* (LvSRT) was performed using the protocols described earlier²². Briefly, the full length sequence was cloned into Novagen's pET14b vector system and transformed into *E. coli* strain BL21(DE3). Recombinant SRT expression was achieved with a purity of ~90% and an estimated yield of ~50 mg/L. The yield increases approximately ten fold (i.e., ~0.5 g/L) in auto induction media. The size of the protein was confirmed via an SDS-page gel (**Fig. 2d**).

WGM resonator fabrication: Details on the Si master preparation and etching for micro-WGM fabrication were reported earlier³³. Briefly, the microtoroids were fabricated from a 2 μm thick oxide layer on a silicon wafer. First, series of circular pads of 80 μm in diameter were created through a combination of standard photolithography technique and buffered HF etching. These circular pads serve as etch mask for isotropic etching of silicon in XeF_2 gas chamber, leaving under-cut silica disks supported by silicon pillar. The microdisks were then selectively reflowed using a 30W carbon dioxide (CO_2) laser to form a toroidal shape. A negative mold was made from polydimethylsiloxane (PDMS, Dow Corning Sylgard® 184 silicone elastomer kit). PDMS

and curing agent were mixed in a 10:1 ratio, stirred and degased under vacuum for 30 minutes. The mix was poured on the silicon master and it was cured at room temperature for 24 hours. Due to mechanical processing requirements (e.g., viscosity in solvent depends on protein molecular size and solubility), the shape and size of WGM resonators varied. SRT microresonators had a major diameter of 54 μm and a minor diameter of 9 μm , which were used in quality factors and dn/dT measurements. For ThT dye experiments, we used larger SRT microresonators (i.e., 100 μm). Silk microresonators had a major diameter of 94 μm and minor diameter of 5 μm .

Protein casting: SRT solution (either recombinant or native protein) was prepared by dissolving 50 mg/mL of protein in hexafluoro-2-propanol (HFIP). The solution was sonicated for 1 hour and vacuum-filtered in a 4-8 μm mesh size filter. 80 μL of SRT solution were poured into a PDMS toroid mold in successive 20 μL additions 1 minute apart. After the last addition, the HFIP was evaporated at room temperature in the fume hood for 5 minutes and the mold-SRT system was immersed in butadiene (plasticizer) at 80°C (above T_g) for 30 minutes. The thermoplastic SRT film was peeled off with tweezers and excess butanediol was removed by rinsing with ethanol. For silk protein solution, we followed the protocol reported earlier⁵. Aqueous silk solution was injected into the PDMS mold and evaporated at room temperature in a desiccator overnight.

WGM / resonance: Taper-fibers fabricated by heating and pulling single mode fibers were used to couple light from a tunable laser into and out of the microtoroid resonators. The coupling distance between the taper and the resonators was controlled by a nanopositioning system. Four tunable lasers with emission in the wavelength bands of 670 nm, 780 nm, 980 nm and 1450 nm were used to characterize the resonators in different bands of the spectrum. Their wavelengths were linearly scanned around resonances of the resonators. The real-time transmission spectra were obtained by a photodetector connected to an oscilloscope. The scanning speeds and powers of the lasers were optimized in order to eliminate thermally-induced (due to heat build-up in high-Q resonators) line-width broadening and narrowing effects. Typical operating conditions for scanning speed and laser power were 10-20 nm/s and 15 μW , respectively.

Mechanical characterization: Protein films were prepared by casting 50 mg/mL SRT/HFIP solution or Silk/H₂O on PDMS molds, resulting in 40x8x0.03 mm rectangular films (length, width, thickness). The samples were analyzed in a dynamic mechanical analysis instrument (TA 800Q DMA) with a three-point bending clamp of 20 mm length between supports. Strain ramp experiments were performed at room temperature at a rate of 250 μ m/min with a preload of 0.02 N. The flexural modulus was calculated as described in ASTM D790 – 10.

Fluorescence imaging: Thioflavin-T (Sigma) aqueous solution is prepared at 0.125 μ M concentration. The absorbance and emission spectra are measured using a fluorescence microscope (Zeiss LSM 5 PASCAL system coupled to a Zeiss Axiovert 200M microscope) at 458 nm wavelength.

SRT fibers: Fibers were obtained through an electrospinning process that utilized a conventional horizontal setup from Dr. Seong Kim's laboratory at the Pennsylvania State University. The schematic design consisted of three components (**Fig. S6**): a syringe for supplying the SRT solution, a collecting platform for accumulating the array of fibers, and a voltage source for generating the necessary electric field. A standard procedure began with the preparation of an approximately 50 mg/mL solution of SRT in hexafluoro-2-propanol (HFIP). Once fully dissolved, 0.5 mL of the solution was drawn into the 1 cm diameter plastic syringe, whose 22 gauge bevel tip needle was previously cut perpendicularly to its cylindrical axis, straightening the eventual orientation of the fiber jet. Placing the syringe securely in the pumping device (PHD 2000 Programmable, Harvard Apparatus, Holliston, MA) contained in the ventilation hood, the collecting platform was then configured. Supported by a ring stand and clamps, the collecting platform, constructed from cut pieces of aluminum held 0.8 cm apart by glass slides and epoxy, was positioned such that its center was aligned with the syringe needle, 6.5 cm away from the tip. With the setup complete, the syringe needle was attached to the 10 kV source (HV Power Supply, Gamma High Voltage Research, Ormond Beach, FL), and the aluminum plates of the collecting platform were grounded. After establishing the voltage difference, the pumping device was activated with an infusion rate of 250 μ L/min. Following the discharge of approximately 0.25 mL of the solution, the pumping process was terminated and the voltage

source detached. To ensure that the HFIP evaporated completely, five minutes were allowed for drying, and the collecting platform was then removed and inspected for fibers between its plates.

Pump-probe transient absorption measurements: A Ti:sapphire laser (Spectra-Physics, Tsunami) is used for time domain transmissivity measurements. Laser characteristics were 800 nm central wavelength, 10 nm bandwidth, 90 fs pulse duration, and 80 MHz repetition rate. The beam is split into two paths (pump and probe paths) by a polarizing beam splitter (PBS) and the pump is frequency doubled to 400 nm wavelength, pump: 7.5 mW (average power of pump modulated at 10 MHz using a sinusoidal envelope), probe: 2.5 mW of average power. The beam size 17 micron for the probe and 35 micron for the pump with synchronous sampling via mechanical delay stage. The transmittance signal is digitalized using a Thorlabs DET10A Si Detector and a Zurich Instruments UHFLI digital lock-in amplifier. The resulting voltage is on the order of 10^{-6} V; data was collected up to pump-probe time delays of 5.5 ns, with variation and noise of 1 nV and 0.2 μ V respectively. The bandwidth of the detector was 1 GHz. The delay between pump and probe is mechanically controlled using Newport Optical Delay Line Kit. A combination of LabView and MatLab programs (developed in-house at the ExSiTE Lab, UVa) were used to analyze the data.

Acknowledgments

MCD, AP, HJ and RS were supported by the Office of Naval Research under grant No. N000141310595, Army Research Office under grant No. W911NF-16-1-0019, and Materials Research Institute of the Pennsylvania State University. LY, SKO, and HY were supported by the Army Research Office under grant No. W911NF-12-1-0026 and the National Science Foundation under grant No 1264997. PEH and CJS were supported by the Air Force Office of Scientific Research under grant No. FA9550-15-1-0079 and Army Research Office under grant No. 151630-101-GG11945-31345. We thank Dr. Seong Kim, Mr. Steven Huang, and Mr. Linhua Xu for providing electro-spinning set up, helping in optical set up and thermo-optic coefficient of silk data respectively.

Author contributions

MCD and ŞKÖ conceived the idea and planned the research. MCD derived structure-property equations. MCD, ŞKÖ, PH and LY supervised the research. HY fabricated the resonators and performed the photonics measurements and data analysis. AP performed the mechanical and spectroscopic measurements and data analysis. CS and PH performed the pump-probe transient absorption measurements. RS prepared the fibers and HJ worked on the cloning, recombinant expression and purification of structural proteins. All authors contributed to writing and revising the manuscript, and agreed on the final content of the manuscript.

Additional information

The authors declare no competing financial interests. Supplementary information accompanies this paper on www.nature.com/naturephotonics. Reprints and permissions information is available online at <http://npg.nature.com/reprintsandpermissions>. Correspondence and requests for materials should be addressed to MCD, ŞKÖ and LY.

References

- 1 Berger, O. *et al.* Light-emitting self-assembled peptide nucleic acids exhibit both stacking interactions and Watson–Crick base pairing. *Nature Nanotechnology* **10**, 353-360 (2015).
- 2 Hanczyc, P., Samoc, M. & Norden, B. Multiphoton absorption in amyloid protein fibres. *Nature Photonics* **7**, 969-972 (2013).
- 3 Guerboukha, H., Yan, G., Skorobogata, O. & Skorobogatiy, M. Silk foam terahertz waveguides. *Advanced Optical Materials* **2**, 1181-1192 (2014).
- 4 Huby, N. *et al.* Native spider silk as a biological optical fiber. *Applied Physics Letters* **102**, 123702 (2013).
- 5 Kim, S. *et al.* Silk inverse opals. *Nature Photonics* **6**, 818-823 (2012).
- 6 Santiago-Cordoba, M. A., Boriskina, S. V., Vollmer, F. & Demirel, M. C. Nanoparticle-based protein detection by optical shift of a resonant microcavity. *Applied Physics Letters* **99**, 073701 (2011).
- 7 Santiago-Cordoba, M. A., Cetinkaya, M., Boriskina, S. V., Vollmer, F. & Demirel, M. C. Ultrasensitive detection of a protein by optical trapping in a photonic - plasmonic microcavity. *Journal of Biophotonics* **5**, 629-638 (2012).
- 8 Lu, T. *et al.* High sensitivity nanoparticle detection using optical microcavities. *Proc. Natl. Acad. Sci. U.S.A.* **108**, 5976-5979 (2011).
- 9 Vollmer, F., Arnold, S. & Keng, D. Single virus detection from the reactive shift of a whispering-gallery mode. *Proc. Natl. Acad. Sci. U.S.A.* **105**, 20701-20704 (2008).
- 10 Spillane, S., Kippenberg, T., Painter, O. & Vahala, K. Ideality in a fiber-taper-coupled microresonator system for application to cavity quantum electrodynamics. *Physical Review Letters* **91**, 043902 (2003).
- 11 Aspelmeyer, M., Kippenberg, T. J. & Marquardt, F. Cavity optomechanics. *Reviews of Modern Physics* **86**, 1391 (2014).
- 12 Peng, B. *et al.* Parity-time-symmetric whispering-gallery microcavities. *Nature Physics* **10**, 394-398 (2014).
- 13 Armani, D., Kippenberg, T., Spillane, S. & Vahala, K. Ultra-high-Q toroid microcavity on a chip. *Nature* **421**, 925-928 (2003).
- 14 Borselli, M., Johnson, T. & Painter, O. Beyond the Rayleigh scattering limit in high-Q silicon microdisks: theory and experiment. *Optics Express* **13**, 1515-1530 (2005).
- 15 Barclay, P. E., Srinivasan, K., Painter, O., Lev, B. & Mabuchi, H. Integration of fiber-coupled high-Q SiN x microdisks with atom chips. *Applied Physics Letters* **89**, 131108-131108-131103 (2006).
- 16 Hu, J. *et al.* Flexible integrated photonics: where materials, mechanics and optics meet. *Optical Materials Express* **3**, 1313-1331 (2013).
- 17 Schwesyg, J. R., Beckmann, T., Zimmermann, A. S., Buse, K. & Haertle, D. Fabrication and characterization of whispering-gallery-mode resonators made of polymers. *Optics Express* **17**, 2573-2578 (2009).
- 18 Li, B.-B. *et al.* On chip, high-sensitivity thermal sensor based on high-Q polydimethylsiloxane-coated microresonator. *Applied Physics Letters* **96**, 251109 (2010).
- 19 Monifi, F., Odemir, S. K., Friedlein, J. & Yang, L. Encapsulation of a fiber taper coupled microtoroid resonator in a polymer matrix. *Photonics Technology Letters, IEEE* **25**, 1458-1461 (2013).

- 20 Özdemir, Ş. K. *et al.* Highly sensitive detection of nanoparticles with a self-referenced and self-heterodyned whispering-gallery Raman microlaser. *Proceedings of the National Academy of Sciences* **111**, E3836-E3844 (2014).
- 21 Demirel, M. C., Cetinkaya, M., Pena - Francesch, A. & Jung, H. Recent Advances in Nanoscale Bioinspired Materials. *Macromolecular Bioscience* **15**, 300-311 (2015).
- 22 Pena-Francesch, A. *et al.* Materials Fabrication From Native and Recombinant Thermoplastic Squid Proteins. *Advanced Functional Materials* **24**, 7393-7401 (2014).
- 23 Jung, H. *et al.* Molecular tandem repeat strategy for elucidating mechanical properties of high-strength proteins. *Proceedings of the National Academy of Sciences*, 201521645 (2016).
- 24 Lefèvre, T., Rousseau, M.-E. & Pézolet, M. Protein secondary structure and orientation in silk as revealed by Raman spectromicroscopy. *Biophysical Journal* **92**, 2885-2895 (2007).
- 25 Rogers, D. Screening for amyloid with the thioflavin-t fluorescent method. *American Journal of Clinical Pathology* **44**, 59-61 (1965).
- 26 Ho, C. Y. & Taylor, R. E. *Thermal Expansion of Solids*. (ASM International, 1998).
- 27 Gosline, J. M., Denny, M. W. & DeMont, M. E. Spider silk as rubber. *Nature* **309**, 551-552 (1984).
- 28 Zhang, Z., Zhao, P., Lin, P. & Sun, F. Thermo-optic coefficients of polymers for optical waveguide applications. *Polymer* **47**, 4893-4896 (2006).
- 29 Gorham, C. S. *et al.* Ion irradiation of the native oxide/silicon surface increases the thermal boundary conductance across aluminum/silicon interfaces. *Physical Review B* **90**, 024301 (2014).
- 30 Cahill, D. G. Analysis of heat flow in layered structures for time-domain thermoreflectance. *Review of Scientific Instruments* **75**, 5119-5122 (2004).
- 31 Chou, S. S. *et al.* Chemically Exfoliated MoS₂ as Near - Infrared Photothermal Agents. *Angewandte Chemie* **125**, 4254-4258 (2013).
- 32 Hopkins, P. E. Influence of electron-boundary scattering on thermoreflectance calculations after intra-and interband transitions induced by short-pulsed laser absorption. *Physical Review B* **81**, 035413 (2010).
- 33 Zhu, J. G. *et al.* On-chip single nanoparticle detection and sizing by mode splitting in an ultrahigh-Q microresonator. *Nature Photonics* **4**, 46-49 (2010).